Development of catalytic ceramic filter candles for tar conversion

Grazyna Straczewski [a],[*], Kengo Koutera [a], Uta Gerhards [b], Krassimir Garbev [a], Hans Leibold [a]

[a] Institute for Technical Chemistry, Karlsruhe Institute of Technology, Hermann-von-Helmholtz-Platz 1, 76344 Eggenstein-Leopoldshafen, Germany
[b] Institute for Micro Process Engineering, Karlsruhe Institute of Technology, Hermann-von-Helmholtz-Platz 1, 76344 Eggenstein-Leopoldshafen, Germany

ARTICLE INFO

ABSTRACT

A catalyst with a high activity in tar conversion, impregnated on the ceramic hot gas filter material was developed. The aim of the experiments was to estimate the light-off temperature of the catalytic filter elements for naphthalene (tar model compounds) conversion and the long-term catalytic stability at a temperature of 700 °C. Configuration of the catalyst was optimized through improvements in coking resistance and long-term stability. The composition and morphology parameters of the filter material were considered. Both the impregnation methods and the composition of the impregnation solution were investigated and validated. The catalyst composed of Ni, Fe, Cr oxides, promoted with Pt (AlSi-Cat43-Pt), and impregnated on the ceramic-fiber filter composed of $Al_2O_3(44\%)/SiO_2(56\%)$ was found to be the most active catalyst. The designated catalyst was catalytically active at temperatures of about 700 °C, with a naphthalene conversion of around 93% over 95 h without catalyst deactivation. We found that the steam and gas compositions had an influence on the catalytic activity of the filter elements. The same catalytic filter was catalytically active for 115 h at a low concentration of H_2O (10 vol%) and H_2 (3 vol%) with a naphthalene conversion of 98% at 790 °C without significant deactivation.

1. Introduction

Biomass gasification, which is one of the technologies for the thermochemical conversion of biomass, is expected to be the key to the spreading of small and medium-sized biomass power plants around the world. In order to extract energy from biomass efficiently and cost-effectively, a large-scale "biomass combustion plant" is used, which converts biomass into heat in the boiler and generates electricity in the boiler steam turbine by generating steam. A significant restriction of biomass gasification is mainly caused by the incomplete biomass gasification process resulting in the formation of numerous contaminants. These impurities include particulate matter (i.e., coal, carbon black), condensable polycyclic aromatic hydrocarbons called tar, sulfur compounds, nitrogen compounds, alkali metal, and hydrogen chloride [1]. Among the contaminations that should be eliminated, tars and particles are the most important, as they cause clogging of the pipes and the gas engine, which is the biggest technical problem of biomass gasification and leads to the inefficiency of the plant [2]. In gas purification, particle cleaning is almost entirely based on one or more of the following principles: inertial separation, barrier filtration, and electrostatic precipitation [3]. On the other hand, the development of tar cleaning technology must be continued. The method of tar cleansing is divided into two groups i.e., tar removal and tar conversion. Treatments inside the gasifier are called primary methods. An ideal primary-method concept eliminates the use of secondary treatments. The major issues include (a) the proper selection of gasification conditions (thermal cracking), (b) the use of suitable bed additives or catalysts during gasification, and (c) a suitable gasifier design. In every respect, the gasification conditions play a very important role in the gasification of biomass, but the choice of parameters depends on the type of gasifier [4]. However, the primary process cannot prevent the beneficial gas composition and heating value from being affected, because part of the production gas is burned during the primary tar removal process [5,6]. Treatments outside the gasifier are referred to as secondary methods. The gas from the gasifier is typically conditioned downstream of the gasifier in a secondary reactor. Catalytic conversion has the potential of reducing the thermal and economic impacts of high-temperature operation, as additional energy input may not be required and thermodynamic efficiency losses can be minimized [6]. In addition, the energy content of the tars can be made available by catalytic conversion.

In the present biomass gasification plant using secondary catalytic tar purification, tar removal and conversion respectively and particle removal are carried out separately, which means that the plant can be more compact when processes are carried out in the

* Corresponding author.
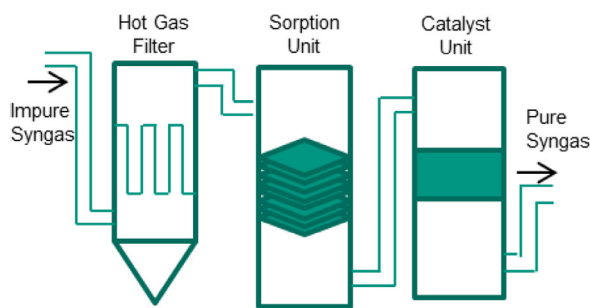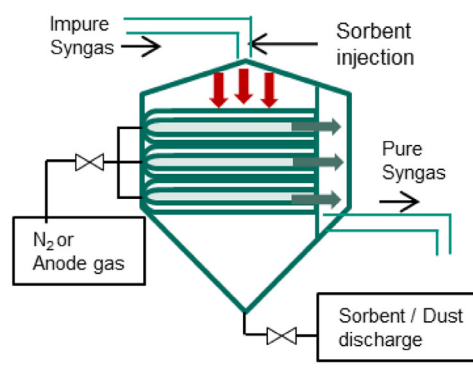 E-mail address: grazyna.straczewski@kit.edu (G. Straczewski).

Fig. 1. Gas cleaning unit in a conventional biomass gasification plant (left) and a compact biomass gasification plant (right).

same reactor. Catalytic filters can combine the two tasks of solid-state filtration and tar conversion in one process step. Impregnation of the filter element with is accomplished by either (a) applying a catalytic coating, (b) adding the catalytic component to the structure of the filter, i.e. the mixture of ceramic grain and binder, or (c) use of a porous inner tube attached to the head of the candle to allow integration of a catalyst particle layer [6]. Nacken et al. [7] developed the catalytic filter element on the basis of a catalyst particle layer with a particle size fraction between 0.1 and 0.3 mm, followed by method (c). They achieved the catalytic activity of Mg6Ni (S) (6 wt% Ni, MgO-supported catalyst) for 100 h at 800 °C with a filtration rate of 90 m h^{-1} (2.5 cm s^{-1}) in the presence of 100 ppmv H$_2$S, with complete conversion of naphthalene. Zhang et al. [8] used α-Al$_2$O$_3$-based filter discs as a model of candle filter, and benzene as a model of tar compound, respectively. They developed the nickel-activated catalytic filter (1 wt% Ni + 0.1, 0.5 or 1.0 wt% CaO, CaO was used as a promoter for the resistance to sulfur poisoning), using a urea precipitation process, which is categorized into method (b). Studies have been conducted to improve the optimal Ni/CaO ratio for the sulfur resistance of the nickel- activated catalytic filter. Although experiments were monitored for at least 60 min after the reaction had reached an apparent steady state, a benzene conversion of 93% (50 ppm H$_2$S) and 78% (100 ppm H$_2$S) was achieved at a filtration gas velocity of 2.5 cm s^{-1}.

This study was part of a project, which aims to develop an "energy-saving compact catalytic hot-gas cleaning unit" for increasing the share of electricity. The key components of the gas cleaning unit in this project were the low-cost entrained-flow sorption process and the catalytic candle filter inside the reactor. Whereas alkali, HCl, H$_2$S, etc. in the raw gas will be removed by the sorption process, particulates and tars will be eliminated and converted. These key components provide elimination of syngas impurities in only one device and make the entire gasification process more compact than conventional reactors of biomass gasification plants (Fig. 1).

The current investigation focuses on the development of a catalytic candle filter that can remove the particulates in the product gas on its filter side (outside) and can convert tars into smaller organic compounds on its catalyst side (inside) (Fig. 2). The catalytic candle filter has to be active in the long-term at temperatures of about 700 °C.

Moreover the coating method regarding the optimal impregnation procedure for the ceramic candle and the strategy for long-term stability with in-situ regeneration of the catalyst were realized. Initially the catalytic elements Ni, Fe, Cr, and Mn were selected and impregnated on the filter discs. We have chosen these metal elements for many reasons. Nickel is known as the most ef-
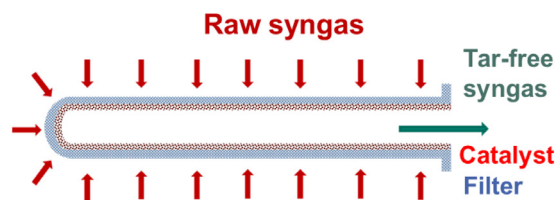

Fig. 2. Catalytic candle filter.

fective and reasonable catalyst for tar steam reforming [9,10]. Ni and Fe are also effective for NH$_3$ conversion [3]. Cr and Mn can reduce coke on the surface of the catalyst, which is generated during the tar conversion [11,12]. In addition, a small amount of Pt or Ru and, for some samples, both noble metals were placed in filter discs so that the catalyst will already be effective at lower temperatures. In particular, Pt is well-known as a strong catalyst in the temperature range below 500 °C [13].

2. Experimental

2.1. Support materials

Two types of filter discs were chosen as support materials: an Al$_2$O$_3$ (44%)/SiO$_2$ (56%) fiber composite manufactured by Rath, and an Al$_2$O$_3$ fibers/SiC grains material with a porosity of 35~38% manufactured by Pall. In the following, the materials are denoted as AlSi and SiC, respectively. The Al$_2$O$_3$/SiC support material has a black SiC side without Al$_2$O$_3$ coating and a white membrane coating on it. The Al$_2$O$_3$/SiO$_2$ disk has no specific side. These disk materials have a diameter of 45–50 mm and a thickness of 10–20 mm. Table 1 gives a comparison of these support materials.

2.2. Catalyst preparation

The catalysts investigated were first prepared on the above support materials. The composition of the catalysts was examined on pellet-type support material and successfully tested for tar conversion [14]. In the next step, an improved catalyst was applied and optimized with regard to coking resistance and long-term stability.

During the first impregnation, metal oxides were generated on the filter discs. All catalysts were combined with the same amounts of Ni (7,2 wt%) and Fe (3,6 wt%) oxides. The contents of Mn and Cr were as follows: 0.35 wt% Cr for Cat43, 3.5 wt% Cr for Cat44, 0.44 wt% Mn for Cat45, and 4.4 wt% Mn for Cat46. 10 ml of each catalytic solution, which contained 4.95 g Ni (NO$_3$)$_2$•6H$_2$O (VWR Chemicals, 99%), 3.6 g Fe (NO$_3$)$_3$•9H$_2$O (VWR Chemicals, 99.9%), and 0.38 g or 3.8 g Cr (NO$_3$)$_3$•9H$_2$O (Fluka, 99%) on the one

Table 1
Comparison of the two support materials.

	AlSi	SiC
Composition	Al_2O_3(44)/SiO_2(56) Fiber composition	SiC grains (body)/Mulite grains (membrane)
Porosity	80 ~ 90%	35 ~ 38%
Pressure Drop	Low	High
Diameter	50 mm	45 mm
Thickness	20 mm	10 mm
Ave. Weight	11.123 g	29.763 g

Table 2
Catalyst name, composition, and preparation method.

SiC−Cat43-Pt	First impregnation: Ni, Fe, Cr(0.35); Second impregnation: Pt
AlSi-Cat43-Pt	First impregnation: Ni, Fe, Cr(0.35); Second impregnation: Pt
SiC−Cat44-Pt	First impregnation: Ni, Fe, Cr(3.5); Second impregnation: Pt
AlSi-Cat44-Pt	First impregnation: Ni, Fe, Cr(3.5); Second impregnation: Pt
SiC−Cat45-Pt	First impregnation: Ni, Fe, Mn(0.44); Second impregnation: Pt
AlSi-Cat45-Pt	First impregnation: Ni, Fe, Mn(0.44); Second impregnation: Pt
SiC−Cat46-Pt	First impregnation: Ni, Fe, Mn(4.4); Second impregnation: Pt
AlSi-Cat46-Pt	First impregnation: Ni, Fe, Mn(4.4); Second impregnation: Pt
AlSi-Cat43-Pt[10]	First impregnation: Ni, Fe, Cr from 10 ml of metals solution; Second impregnation: Pt,
AlSi-Cat43-Pt[20]	First impregnation: Ni, Fe, Cr from 10 ml of metals solution + 10 ml HNO_3 solution (pH 2); Second impregnation: Pt
AlSi-Cat43-Pt[30]	First impregnation: Ni, Fe, Cr from 10 ml of metals solution + 20 ml HNO_3 solution (pH 2); Second impregnation: Pt
AlSi-Cat43-Pt[40]	First impregnation: Ni, Fe, Cr 10 ml of metals solution + 30 ml HNO_3 solution (pH 2); Second impregnation: Pt
AlSi-Cat43-Pt (Ni-Pt)	First impregnation: Fe, Cr; Second impregnation: Ni, Pt
AlSi-Cat43-Pt (Pt-O)	First impregnation: Ni, Fe, Cr; Second impregnation: Pt in EDTA basic solution
AlSi-Cat43-Pt (Pt-Ru)	First impregnation: Ni, Fe, Cr; Second impregnation: Pt, Ru
AlSi-Cat43-Pt (Pt-O-Ru)	First impregnation: Ni, Fe, Cr; Second impregnation: Pt, Ru in EDTA basic solution
AlSi-Cat43-Pt (Pt-HYD)	First impregnation: Ni, Fe, Cr; Second impregnation: Pt in hydrotalcite (HYD) suspension solution

hand, and, on the other hand, 0.27 g or 2.7 g $Mn(NO_3)_2 \bullet 4H_2O$ (Alfa Aesar, 99.98%) dissolved in diluted HNO_3 (pH 2), were dropped onto the surface of two support materials. To distinguish the catalyst samples easily, they were coded with a combination of the name of the support material, the catalyst solution number, and an action symbol (see Table 2). In case that the solution did not at once soak into the support material, the dropping procedure was conducted several times until 10 ml was soaked thoroughly. After the wet impregnation procedure was finished, each catalyst was dried in the oven at around 90 °C overnight and was then calcined at 450 °C for 12 h.

In the second impregnation procedure, noble metal was applied to the filter discs. Pt or Pt-Ru in water solution or basic EDTA solution (0.1 g EDTA in 0.1 mol/l NaOH) and Pt in hydrotalcite suspension (0.01 g in 50 ml H_2O), which contained 25 mg Pt $(NH_3)_4 \bullet Cl_2 \bullet H_2O$ (Alfa Aesar, 99.9%) and/or 40 mg $[Ru(NH_3)_6] \bullet Cl_2$ (Alfa Aesar, 99.9%) (see Table 2), were dropped onto each sample. The volume of Pt solution depended on the weight of the support material itself. The percentage of Pt/Ru in the solution was up to 0.2 wt%. Then, drying and calcination were done under the same conditions as described above.

Three groups of catalytic filter elements were prepared via wet impregnation. In the first group, two different support materials were tested with respect to their compatibility with the impregnation methods and the influence of Cr and Mn on the catalytic activity. In the second group with AlSi as support material, the effect of different impregnation solution concentrations on the catalyst distribution on the support filter material was investigated. In the third group, catalytic filter elements were prepared where the noble metals Pt or Pt-Ru were impregnated using different compositions of the solution.

2.3. Catalyst characterization

For measurement of the Brunnauer-Emmett-Teller (BET) surface area, the catalysts were fragmented and dried for 30 min at 150 °C in ChemiSorb 2750 (Micromeritis) before and after the experiment. Then, the measurement of one catalyst sample was repeated three

times and each catalyst was measured three times. To investigate the surface morphology and the catalyst distribution in the support material, each of the catalysts was analyzed before and after the experiment by SEM (scanning electron microscope) (XL30 ESEM, Philips) and EPMA (electron probe micro analyzer) (JXA-8530F hyperprobe, JEOL), respectively. The catalytic filter samples were also investigated by powder X-ray diffraction (XRD) using MPD Xpert-pro (PANalytical, Almelo, Netherlands) equipped with a multistrip PIXell detector (255chanels, 3.347°2Θ) and Cu radiation. The Cu-Kβ was filtered with Ni filter. The measurements were taken with Soller slits 0.04 rad (2.3°) and adjustable slits giving a constant irradiated sample length of 10 mm. For the purpose of phase identification, the software packages Highscore-Plus (PANalytical) and Diffrac-Plus (Bruker-AXS, Karlsruhe, Germany) combined with PDF 2004 (ICDD) und COD 2019 databases were used.

2.4. Experimental setups

The catalytic tests were performed in a continuously operated stainless steel tubular reactor of 5 cm diameter and 20 cm height mounted inside the hood furnace at space velocities (GHSV) of 8400 and 20,700 h^{-1} (see Fig. 3). For all experiments, except for tests on catalyst behavior at different gas compositions (see Table 3), a gas consisting of 10 vol% CO_2, 10 vol% H_2O, and 0.15 vol% naphthalene as model tar compounds and 79.85 vol% N_2 as carrier gas for steam and naphthalene was used.

The composition of all gasses used was set in the system design software LabVIEW and provided by digital Mass Flow Controllers (MFC, Bronkhorst). Steam was added to the gas by evaporating the water in an electrically heated tank at a temperature of 58 °C or 76 °C. Naphthalene was added by evaporating the solid compound immersed in the oil bath at a constant temperature of 90 °C. All incoming gasses with a volume flow of 0.33 Nm³/h were brought together in a one-meter-long mixing chamber and preheated to 190 °C. The catalytic filter disk with a filter area of 12.6 cm² was placed inside of the tubular reactor with appropriate sealing materials (Isoplan 1000), fixed in the flange, and fastened with screw bolts and hexagon nuts to the tube reactor. Two
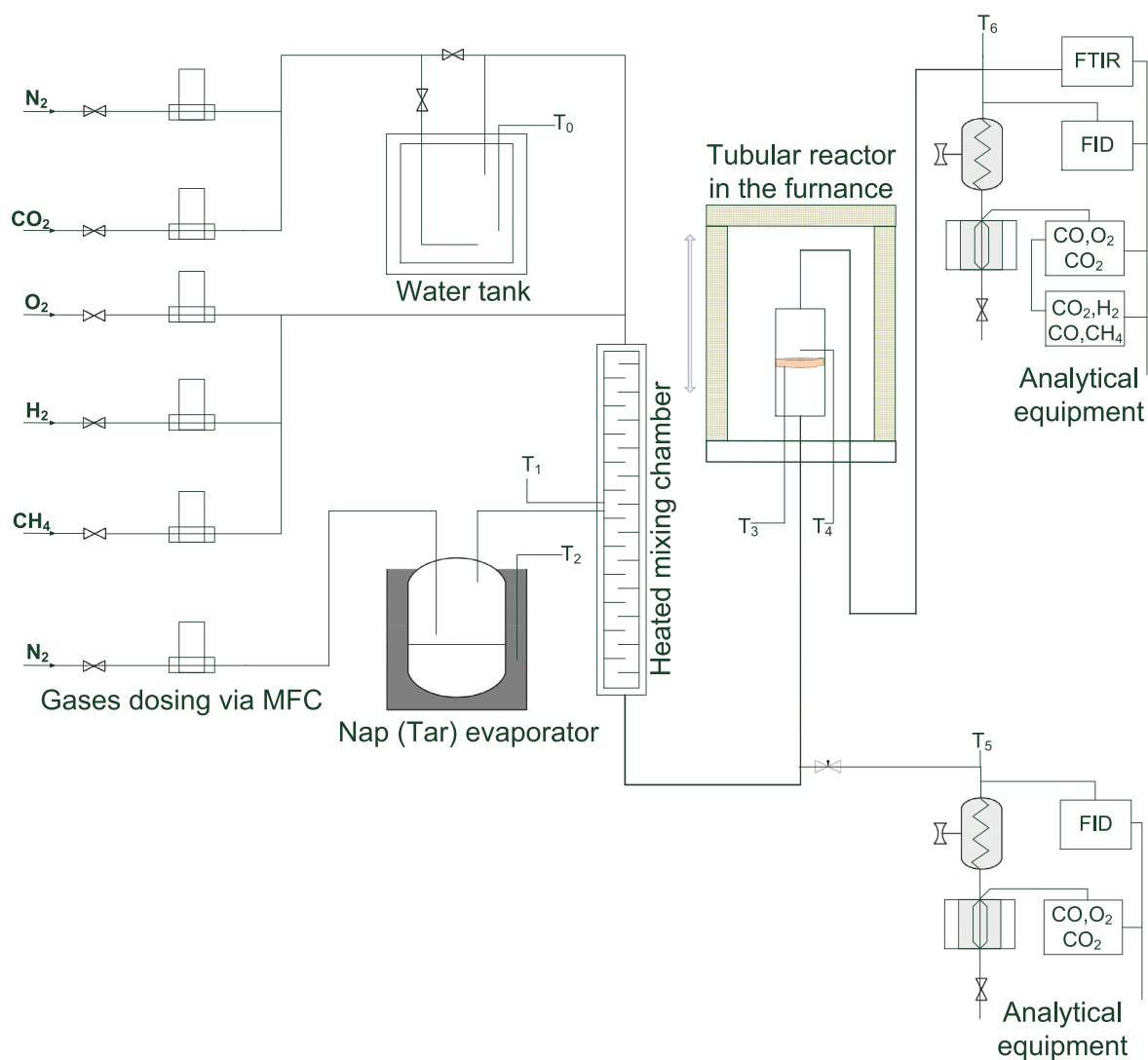
Fig. 3. Design of the DIASPO lab-scale facility.

Table 3
Gas compositions for testing the behavior of the catalyst at various gas component concentrations.

	H_2O [vol%]	CH_4 [vol%]	H_2 [vol%]	CO_2 [vol%]	Nap [vol%]	N_2 [vol%]
A	10	2	3	10	0.15	74.85
B	10	4	15	10	0.15	60.85
C	25	2	3	10	0.15	59.85
D	25	4	15	10	0.15	45.85

thermocouples on the top and bottom of the filter disk measured the temperature inside the reactor. In order to avoid condensation of the naphthalene and its decomposition products, all pipe joints were heated in a controlled manner (standard heaters: WiNKLER, IsoPad, HORST, Hillesheim) or covered with thermal insulation materials. Both raw and reformed gas mixtures were analyzed by an on-line modular detection system. The total concentration of hydrocarbons was measured with a flame ionization detector (FID, Ultramat 5, Siemens). CO, CO_2, and O_2 were measured after cooling in the Cooler EC (M & C) with an infrared analyzer (IR Ultramat 23, Siemens). The concentrations of detectable organic and inorganic compounds after the reaction during the long-term measurements were detected and measured using a Fourier Transform Infrared Spectrometer analyzer (FTIR, Gasmet Technologies) by means of the software Calcmet (Gasmet Technologies).

2.5. Experimental performance

Two kinds of experiments ("catalyst light-off temperature" and "long-term catalytic activity") were performed at the DI-ASPO test facility with two groups of catalytic filter elements: Catalysts on two different support materials (SiC–Cat43-Pt, AlSi-Cat43-Pt, SiC–Cat44-Pt, AlSi-Cat44-Pt, SiC–Cat45-Pt, AlSi-Cat45-Pt, SiC–Cat46-Pt, AlSi-Cat46-Pt) and catalysts with different noble-metal formulations (AlSi-Cat43-Pt (Ni-Pt), AlSi-Cat43-Pt (Pt-O), AlSi-Cat43-Pt (Pt-Ru), AlSi-Cat43-Pt (Pt-O-Ru), AlSi-Cat43-Pt (Pt-HYD)) were tested. These experiments were carried out during the ramping phase from 300 °C to 650 °C or 850 °C (the average temperature of the reactor inside the furnace was in the range of 570 °C and 790 °C) at 3 °C/min to investigate the catalyst light-off temperature and at 650 °C or 860 °C, respectively for 9–12 h
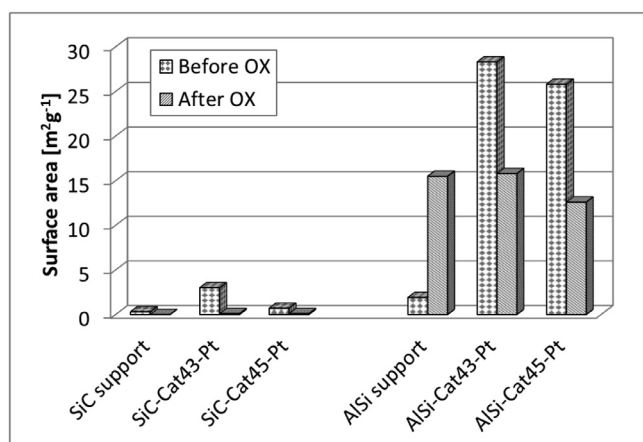
Fig. 4. BET surface area of the catalysts on two different support materials before and after reaction.

(naphthalene reforming) to investigate the long-term catalytic activity. For each catalyst, five or eight heating cycles with long-term naphthalene reforming were conducted. Thus, the tested catalysts were operated for a total of at least 115 h.

The experiments on the catalytic filter discs were conducted intermittently for safety. Thus, the temperature of the furnace was cooled down from 650 °C or 850 °C to 300 °C and kept at 300 °C every night. During the cooling down and keeping of the temperature, the gas flow was changed to only N_2 (0.3 Nm³/h).

3. Results and discussion

3.1. Catalyst morphology

3.1.1. BET surface area

The results of the BET surface area reflect the adsorption capacities of the respective materials. The high surface area, i.e. the high adsorption capacity of the supported catalyst, determines the high affinity to tar conversion reactions of the catalyst.

As shown in Fig. 4, AlSi-supported catalysts before and after naphthalene reforming (Ox) had much better sorption abilities than SiC-supported ones. The initial values of the surface area of SiC support material before and after naphthalene reforming were not detected well. In addition, the change in the surface area between SiC support material and SiC-supported catalysts was small compared to the increase in the case of AlSi. This can be explained by the dense SiC support material with a low porosity (35~38%), and by the wet impregnation method, which was not the optimal method for this material. Moreover, it was considered that there was a limitation in the detection capability of the BET instrument. The maximum value of the surface area of the SiC-supported catalysts was only 3.0 m^2/g for SiC-43-Pt. On the other hand, the surface area of AlSi-supported catalysts was about 14–18 times larger than that of the AlSi support material (1.9 m^2/g), which, in addition, has a much higher porosity (80~90%). Unlike the SiC support material, the surface area of the AlSi support material even slightly increased after naphthalene reforming (AlSi-Cat43-Pt). This can be explained by the adsorption of the reaction products during the experiment [15].

On the other hand, for both catalysts on two different supports, the surface area decreased after naphthalene reforming. It can be assumed that organic compounds and coke derived from tar conversion were adsorbed during the experiment, which reduced the surface area of the working catalysts [16–17]. Nevertheless, this result shows that AlSi as a support material for the catalyst is more suitable than SiC in terms of adsorption capacity.

The BET surface area was also measured and compared for all samples with regard to the catalytic activity of the catalytic filter elements. In all cases, a decrease in the surface area of about 40% after naphthalene reforming was found. The small catalytic filter elements were black-brown. Coke deposits may be responsible for this dark color, but the deposition of organic compounds (reaction products), which were captured between layers of fiber material cannot be excluded either.

3.1.2. EPMA and SEM analysis

In addition to the adsorption capability, the distribution of the catalytic components inside the support materials must be analyzed to evaluate the best impregnation method of the catalysts. The distribution of catalysts on two different supports was estimated with EPMA analysis and is shown in Fig. 5. Each of the catalytic components was uniformly distributed inside the AlSi support material. In the case of SiC, the catalytic components could not penetrate into the SiC grains, regardless of the side from which the impregnation was carried out. They only remained on the surface and inside the white filter membrane (mullite side) of the SiC support material. This is why the SiC support had a low adsorption capability even though the amount of the catalyst solution was the same as in the case of using AlSi as support material. From this point of view, AlSi is much more suitable as a catalyst support material for this impregnation method than SiC.

The EPMA analysis was used also to estimate the best conditions of a wet impregnation procedure of the catalyst. Impregnation of 10 ml metals solution leads to the deposition of the catalyst on the filtration side but not on the side on which the catalyst was added (filter inside). During the impregnation procedure, the catalytic components along with the solution migrate through all support layers up to the filtration outside (see Fig. 6 (above)). In contrast, impregnation of a solution consisting of 10 ml metals solutions and 30 ml dilute HNO_3 (pH 2) leads to a uniform distribution of the transition metal oxides in the entire filter material (see Fig. 6 (below)) due to slowly and repeated infiltration of the solution. A catalyst distribution mainly on the outer side of the filter will be deactivated very quickly. During operation, the filter cake of dust and sorbent particles will block access to the catalyst [18]. Noble metal, as added during the second impregnation step, is distributed uniformly only inside of the filter element. Thus, it is protected against being blocked by particulates and will be available to the tar compounds. Therefore, it is meant that the wet impregnation of the catalyst should be carried out in two steps, the first impregnation step comprises the application of dilute metals solution and the multiple repetition of the impregnation procedure. The second step implies the application of noble metals to the filter material.

Additionally, SEM pictures were made also of all support filters and catalysts on the filter elements. Thereby, the location and distribution of the catalysts were evaluated with respect to the structure of the filter material. In Fig. 7, the differences concerning the location and the adhesion of the catalyst particles can be clearly seen on two support material specimens. On the SiC, the catalyst particles formed agglomerates, which are mostly located in small edges. On the contrary, on AlSi, small and bigger catalyst particles are uniformly distributed along the fibers of alumina silicate. The distribution of the catalyst without agglomeration of the particles enables best adsorption and reduction of the tar compounds on the catalyst.

3.1.3. XRD analysis

Not only the distribution of the catalyst in the amorphous aluminum silicate material is important, but also the phase composition of the active catalyst itself. Therefore, the crystal structures of the new and used Ni, Fe, and Cr catalysts were identified by XRD
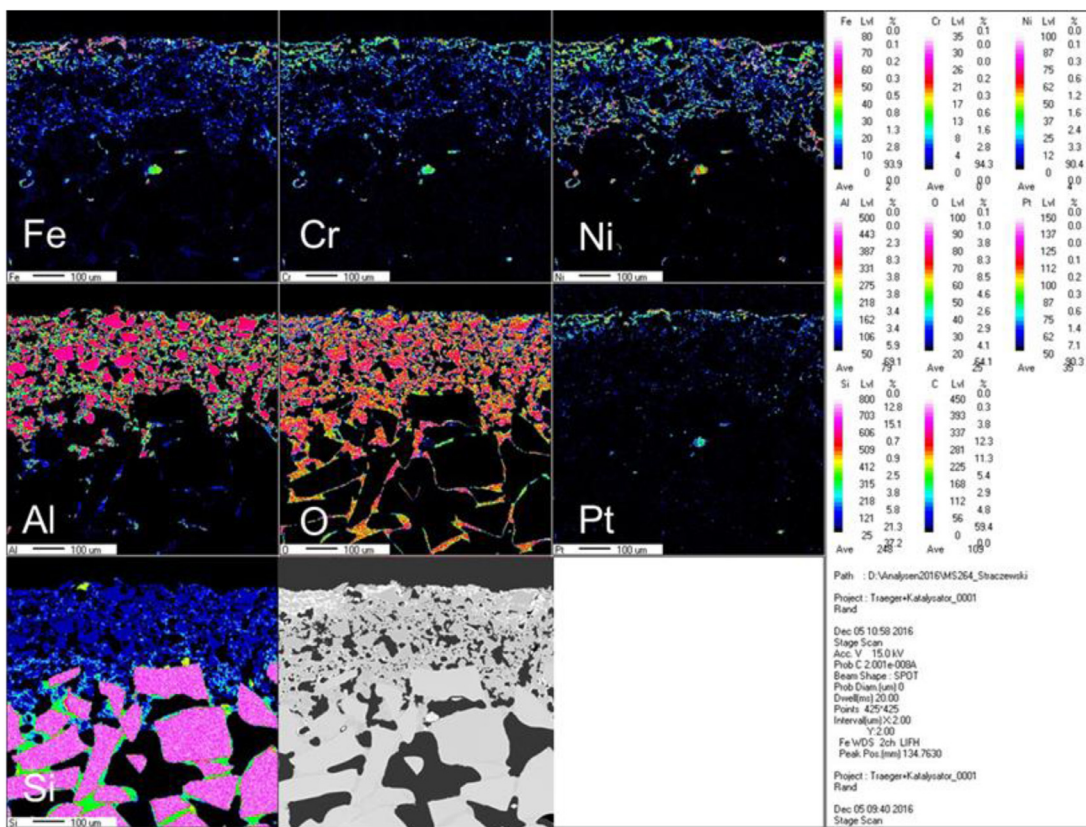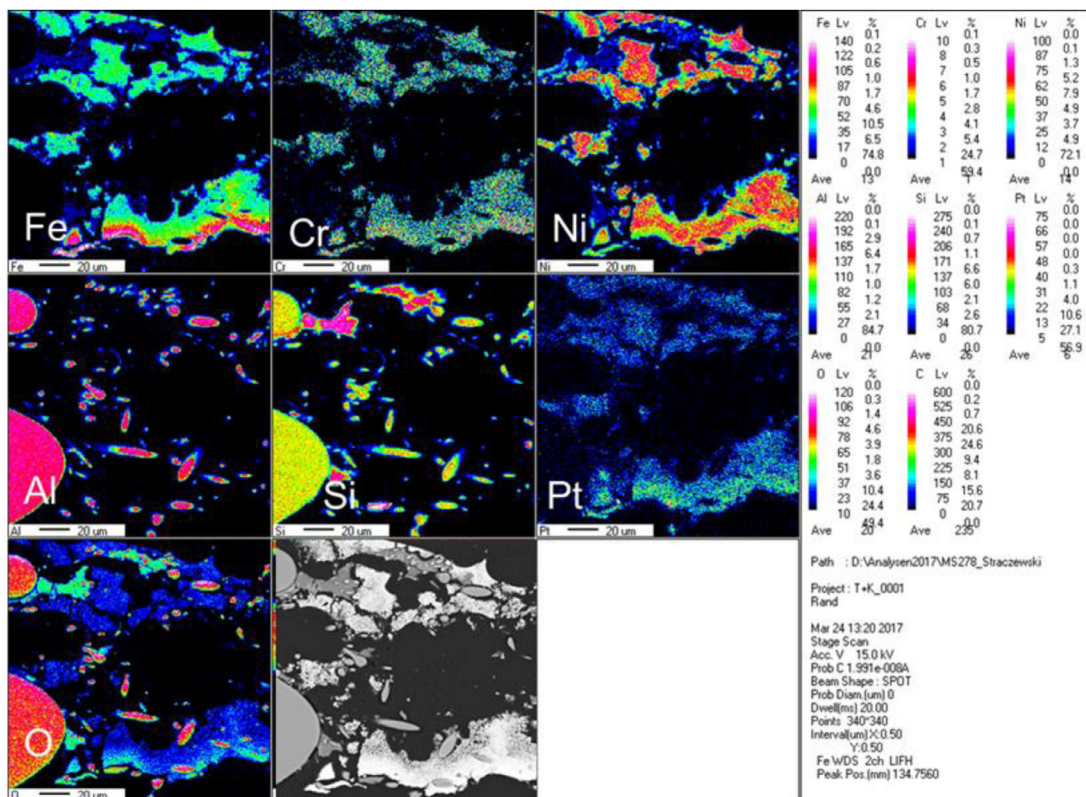
Fig. 5. EPMA (electron probe micro analysis) images of AlSi (above) and SiC (below) related to the respective catalytic components.
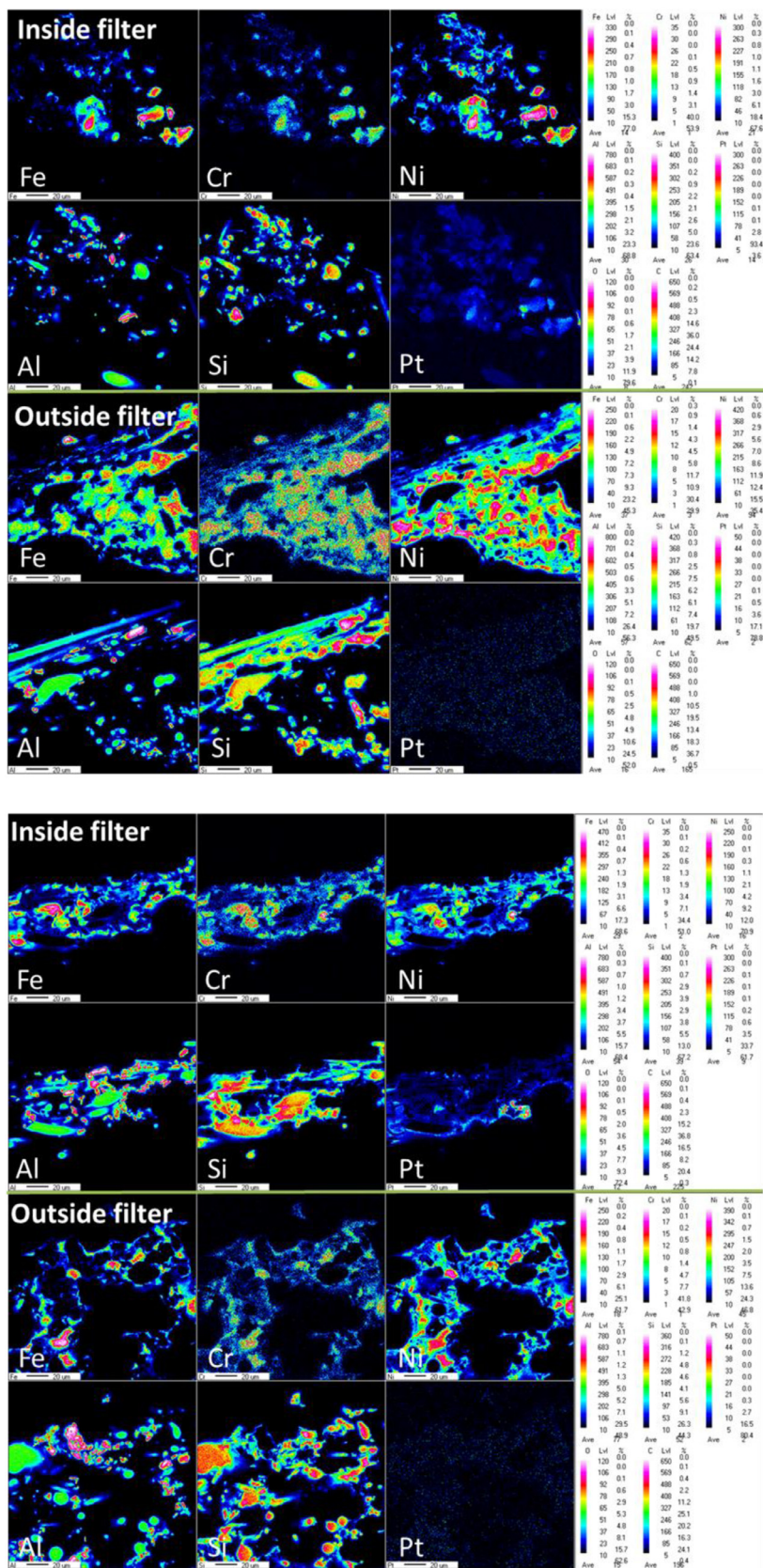
Fig. 6. EPMA images. Above: AlSi-Cat43-Pt[10] catalytic filter elements impregnated with concentrated solution, insi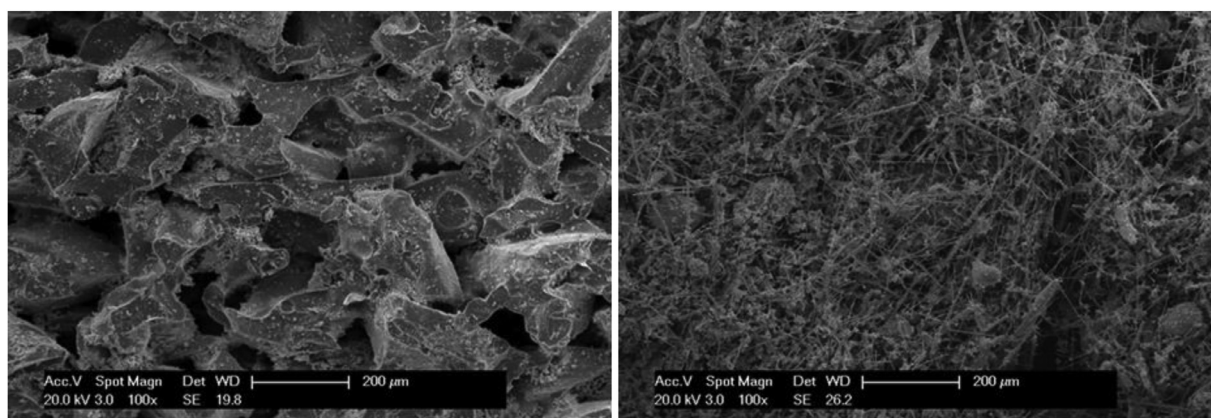de filter (upper picture) and outside filter (lower picture); Below: AlSi-Cat43-Pt[40] catalytic filter elements impregnated with fourfold dilute solution, inside filter (upper picture) and outside filter (lower picture).

Fig. 7. SEM images of SiC−Cat43-Pt (left) and AlSi-Cat43-Pt (right).
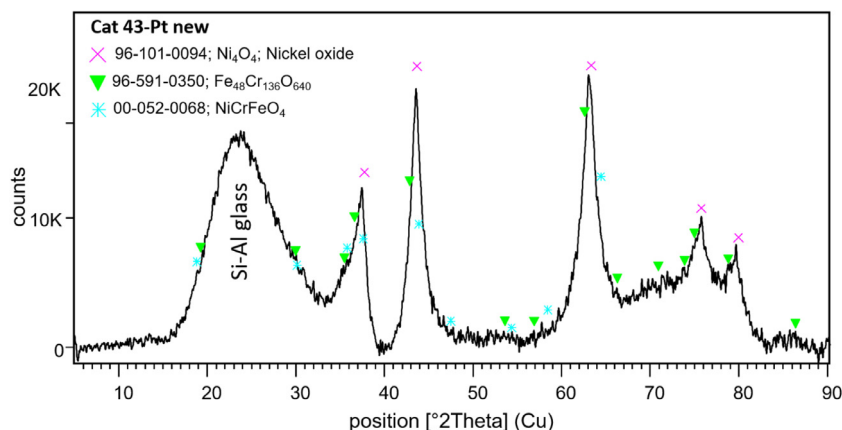

Fig. 8. X-ray diffraction of new Cat43-Pt on amorphous aluminum silicate filter material.
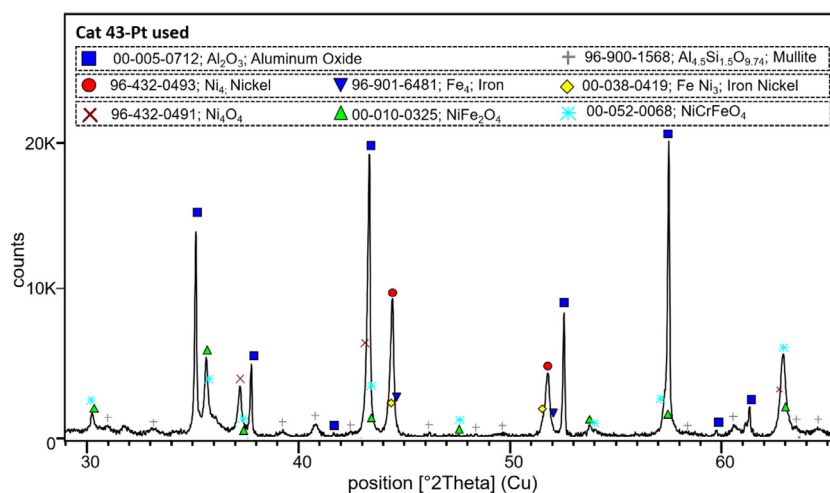

Fig. 9. X-ray diffraction of used Cat43-Pt on amorphous aluminum silicate filter material.

diffraction. As shown in Fig. 8, NiO (2Θ 37.4, 43.39, 63.03, 75.6 and 79.6) dominates in the new catalyst. Its reflections are overlaid on a broad "hump" centered at 23.6 °2Θ which is due to amorphous Si-Al glass substrate. The reflections of NiO (also known as bunsenite) are also broad suggesting a very small crystallite size. In addition, compounds such as iron-chromium oxide and Ni-Cr-Fe oxide mixtures have been identified. After naphthalene reforming, mainly three groups of compounds are recognized in the XRD pattern (Fig. 9): 1) Strong reflections of a-Al_2O_3 accompanied with mulite peaks with low intensity both belonging to the substrate;
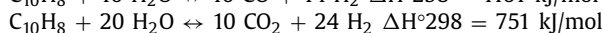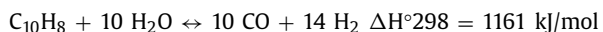
2) metallic Ni (2Θ 44.4 and 51.9) and iron but also mixed metals such as iron nickel and nickel chromium iron; 3) nickel oxide and various mixed metal oxide forms like $NiFe_2O_4$ and $NiCrFeO_4$. The reforming of naphthalene definitely leads to an oxygen loss in the mixed Ni, Fe, and Cr catalyst and thus to an active metal sintering. As a rule, irreversible deactivation of the catalyst can occur. The formation of metallic Ni and catalyst deactivation has also been observed during the methane or propane steam reforming [19,20]. By oxidation of the catalyst with oxygen, the catalyst can only regenerate if the sintering of mixed metals has not yet taken place.

It could not be detected in what form platinum is present in new and used catalysts due to low Pt contents in the catalyst composition.
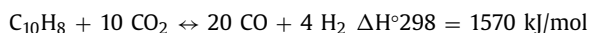
3.2. Catalyst activity

The main reactions that occur during the tar conversion over Ni-based catalyst can be summarized as follows [21,22]:
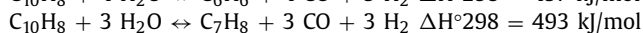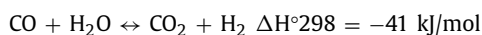
1 Steam reforming

$C_{10}H_8 + 10\ H_2O \leftrightarrow 10\ CO + 14\ H_2$ $\Delta H°298 = 1161$ kJ/mol
$C_{10}H_8 + 20\ H_2O \leftrightarrow 10\ CO_2 + 24\ H_2$ $\Delta H°298 = 751$ kJ/mol

1 Dry reforming

$C_{10}H_8 + 10\ CO_2 \leftrightarrow 20\ CO + 4\ H_2$ $\Delta H°298 = 1570$ kJ/mol

1 Dealkylations

$C_{10}H_8 + 4\ H_2O \leftrightarrow C_6H_6 + 4\ CO + 5\ H_2$ $\Delta H°298 = 457$ kJ/mol
$C_{10}H_8 + 3\ H_2O \leftrightarrow C_7H_8 + 3\ CO + 3\ H_2$ $\Delta H°298 = 493$ kJ/mol

1 Water-gas shift

$CO + H_2O \leftrightarrow CO_2 + H_2$ $\Delta H°298 = -41$ kJ/mol

1 Coke formation

$C_{10}H_8 \leftrightarrow 4\ H_2 + 10\ C$ $\Delta H°298 = -100$ kJ/mol

1 Carbon deposition

$2CO \leftrightarrow C + CO_2$ $\Delta H°298 = -172$ kJ/mol

In these conversion reactions, the composition of the gas coming from the gasifier is an important factor that has a significantly impact on the quantity and quality of the products. The different gas composition leads to different activities and syngases due to different reaction processes. We assume that steam reforming and dry reforming are preferable in our gas composition.

3.2.1. Catalysts on different support filters

The catalytic activities of four catalysts on two different filter materials were tested. The light-off temperatures and long-term activities of these four catalysts were determined in at most three steps in the case of Cat43-Pt and Cat45-Pt catalysts and eight steps in the case of Cat44-Pt and Cat46-Pt catalysts. For these experiments, the value of hydrocarbon conversion (naphthalene and by-products) and the value of naphthalene conversion were determined according to the following equations:

$$X_{CH}(\%) = \frac{C_{CH(in)} - C_{CH(out)}}{C_{CH(in)}} \cdot 100\% \tag{1}$$

$$X_{Nap}(\%) = \frac{C_{Nap(in)} - C_{Nap(out)}}{C_{Nap(in)}} \cdot 100\% \tag{2}$$

where $X_{CH}(\%)$ and $X_{Nap}(\%)$ are the appropriate hydrocarbon conversion and naphthalene conversion rates,%; $C_{CH(in)}$ and $C_{Nap(in)}$ are upstream hydrocarbons or naphthalene concentrations, ppm; $C_{CH(out)}$ und $C_{Nap(out)}$ are downstream hydrocarbons or naphthalene concentrations, ppm.

Compared with the results of pure AlSi or SiC support materials, the effect of the impregnated catalytic components was obvious. Both AlSi-supported catalysts with small contents of Cr and Mn (Cat43-Pt and Cat45-Pt) have shown the same light-off temperature of 460 °C. The respective influences of Cr and Mn could not be detected clearly at this point. Also, in the case of SiC-supported catalysts, the effect of Cr and Mn on catalyst activity could not be determined and the light-off temperature was also 460 °C. The amounts of these individual catalytic components might be too small to detect the difference of these effects. In addition, the different performances of AlSi and SiC could not be clarified by the

comparison of the light-off temperature for these catalysts. Both AlSi-supported catalysts in the long-term activity test at 570 °C were also active for at least 15 h with over 90% of naphthalene conversion (2) (see Fig. 10). Only AlSi-Cat43-Pt could re-activate its catalytic performance after about 20 h of reforming (third heating cycle at 790 °C), but it became deactivated again within a few hours. On the contrary, both catalysts on SiC support suddenly dropped to 50–60% naphthalene conversion after 2 h on stream.

After heating up to 860 °C, the catalysts SiC−Cat43-Pt and SiC−Cat45-Pt showed yet a light-off temperature in the range of 400–500 °C, as shown in Fig. 10, but the CH conversion rate was smaller than during the first reforming cycles. Moreover, the naphthalene conversion rate (2) of SiC−Cat43-Pt and SiC−Cat45-Pt stably achieved about 80% for 10 h, respectively. In the course of the third cycles, the light-off temperatures and the naphthalene conversion rates of two SiC-supported catalysts were tested at up to 650 °C again. The light-off temperature could not be detected anymore. The naphthalene conversion rate of SiC−Cat45-Pt (40%) was higher than in the case of SiC−Cat43-Pt (20%). During the fourth reforming cycle at 790 °C, the light-off temperatures of SiC−Cat43-Pt and SiC−Cat45-Pt were at 650 °C and at 700 °C, respectively. As for the catalytic activity, SiC−Cat 45-Pt achieved a naphthalene conversion of 80% at 860 °C comparable to the second reforming cycle. On the other hand, the naphthalene conversion rate of SiC−Cat43-Pt decreased to around 70%. In that case, the catalyst with Mn seemed to be active for a longer period of time.

As was expected, the catalytic filter discs with higher amounts of Cr and Mn in the catalyst composition (Cat44-Pt and Cat46-Pt) were definitely more active. Nevertheless, the same effect of shifted light-off temperatures was observed (see Fig. 11). Regardless of the support material and catalyst composition in the first heating cycle, the catalysts became catalytically active at temperatures in the range of 450 °C to 480 °C. The dominant effect of Cr or Mn in the activity at the first light-off temperature could not really be recognized. However, the changes in light-off temperatures in the following heating cycle were different for both types of catalysts. In the case of a catalyst with Cr, the light-off temperature was shifted every next heating cycle until it was stabilized at about 700 °C for AlSi-supported catalysts and 640 °C for catalysts on the SiC support. In the case of a catalyst containing Mn, the light-off temperature was suddenly raised to a higher temperature by a second heating cycle. In the next experiments, it remained almost unchanged at approximately 690 °C for the AlSi-supported catalyst and approximately 700 °C for the SiC-supported catalyst. As shown in Fig. 11, both catalysts deactivated at the lower temperature of 580 °C. The Cr-containing catalysts were less active and did not reach more than 80% of the naphthalene conversion (2), but were still active after about 12 h. In contrast, the Mn-containing catalysts were initially more active with naphthalene conversion (2) of about 85–95%, but rapidly lost their activity. In that case, the catalyst on the SiC support was completely deactivated.

After increasing the reactor temperature to 790 °C in the next heating cycle, all AlSi-supported catalysts and all SiC-supported catalysts shifted their light-off temperature (from 440 to 480 °C) to 640–750 °C reaching their full activity again. The naphthalene conversion rate for all these catalysts (AlSi-Cat44-Pt, AlSi-Cat46-Pt, SiC−Cat44-Pt, and SiC−Cat46-Pt) was automatically increased. In general, both types of catalysts were more active on AlSi support filters of about 15% compared to SiC support materials. In this case, also the catalysts containing Cr were more active during the long-term activity measurements. At the beginning of the tests, the catalyst with Mn content (AlSi-Cat46-Pt) was the most powerful in naphthalene conversion, but it began to deactivate after 80 h on stream.

The reason why the catalysts after reforming deactivated at their previous reaction temperature can be related to Pt deactiva-
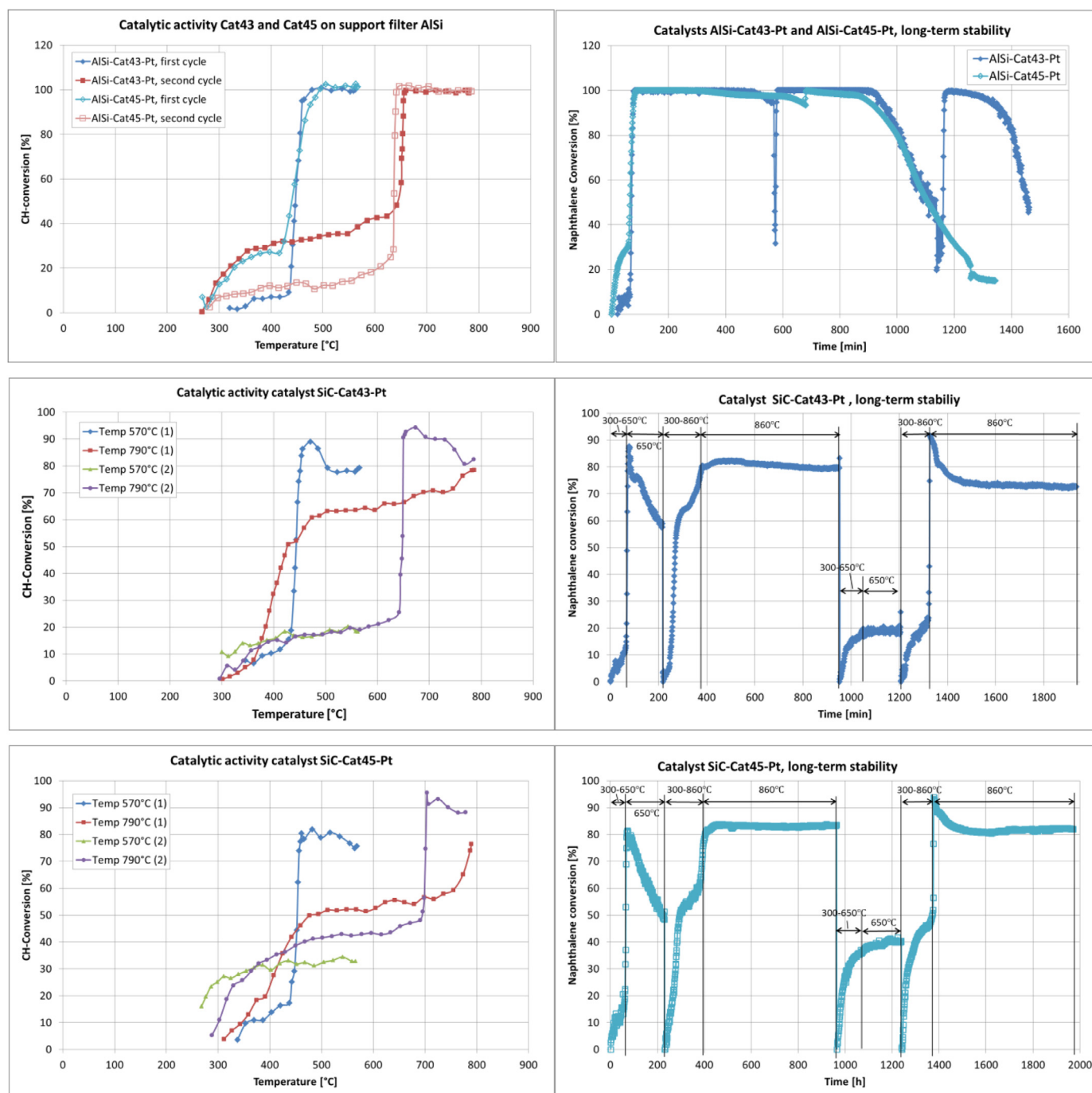
Fig. 10. Hydrocarbon conversion over catalysts: AlSi-Cat43-Pt, AlSi-Cat45-Pt, SiC–Cat43-Pt, SiC–Cat45-Pt, light-off temperature (left), naphthalene conversion at the same catalysts, long-term catalytic activity (right).

tion [16–17,23] and Ni activity. Pt could reduce the reaction temperature of the impregnated catalyst to around 460–540 °C. However, it can be considered that after reforming in this experiment, Pt lost its catalytic activity and then, the reaction temperature was increased to around 630–650 °C but tar conversion occurs at still lower reaction temperature than for typical Ni-based catalysts [24–25].

3.2.2. Catalysts with different noble-metal formulations

In the section above, it was found that Pt, which is responsible for the catalysts´activity at lower temperatures, deactivated during the naphthalene reforming. In this section, it will be examined which influence on the catalysts´activity the platinum or platinum-ruthenium will have if they are impregnated with different solutions (see Table 2, Chapter 2.2). Again, the light-off temperature and the long-term activity of the catalysts (AlSi-Cat43-Pt (Ni-Pt), AlSi-Cat43-Pt (Pt-O), AlSi-Cat43-Pt (Pt-Ru), AlSi-Cat43-Pt (Pt-O-Ru), AlSi-Cat43-Pt (Pt-HYD)) were measured at five or six heating cycles, except for AlSi-Cat43-Pt (Ni-Pt), which was tested only during four heating cycles. The values of the hydrocarbon and naphthalene conversion rates were calculated according to Eqs. (1) and (2). The light-off temperature of the tested catalysts in the initial reforming cycle was between 420 °C for AlSi-Cat43-Pt (Pt-O-Ru) and 485 °C for AlSi-Cat43-Pt (Ni-Pt) (see Fig. 12).
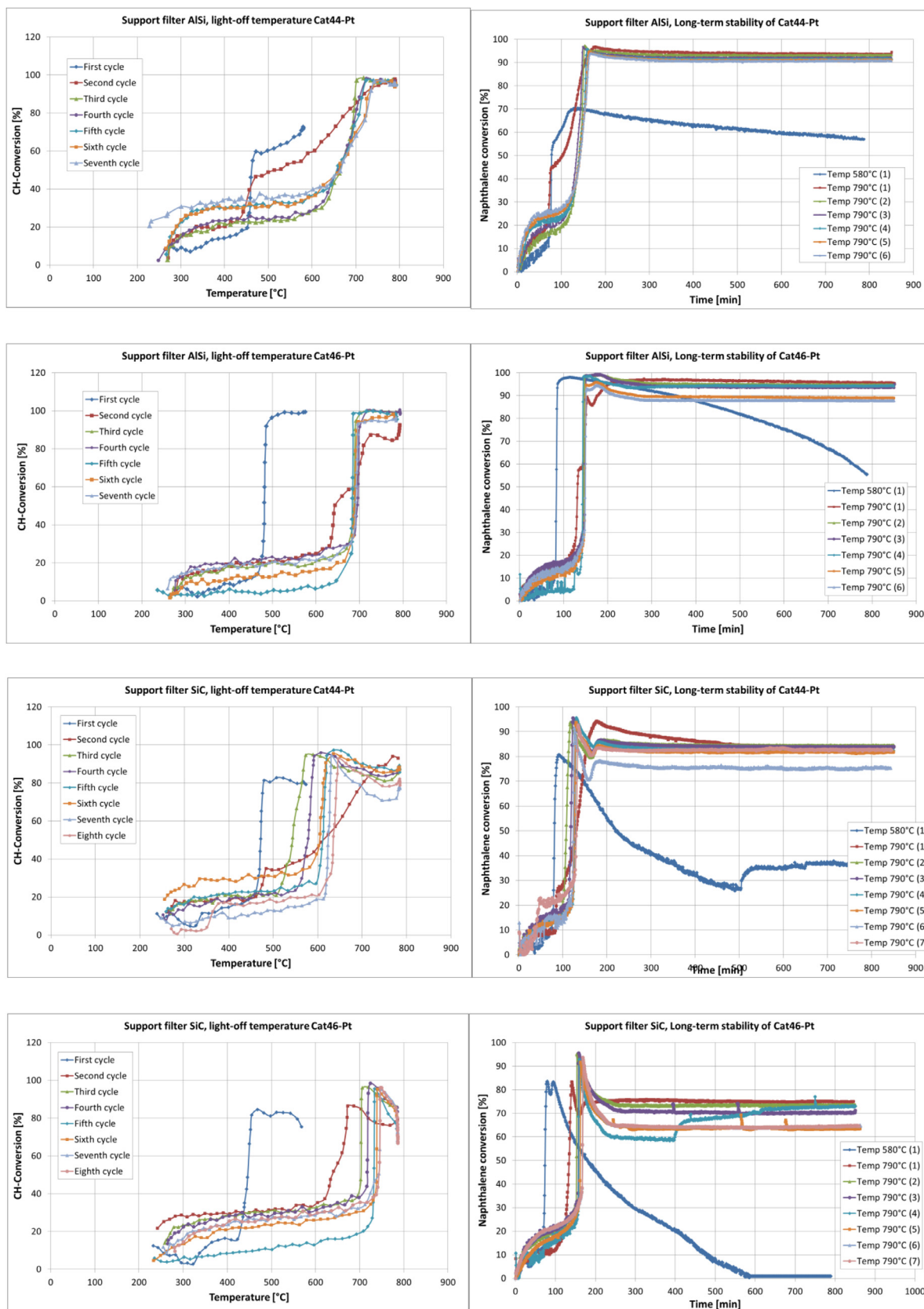
Fig. 11. Hydrocarbon conversion over catalysts: AlSi-Cat44-Pt, AlSi-Cat46-Pt, SiC−Cat44-Pt, SiC−Cat46-Pt, light-off temperature (left), naphthalene conversion at the same catalysts, long-term catalytic activity (right).
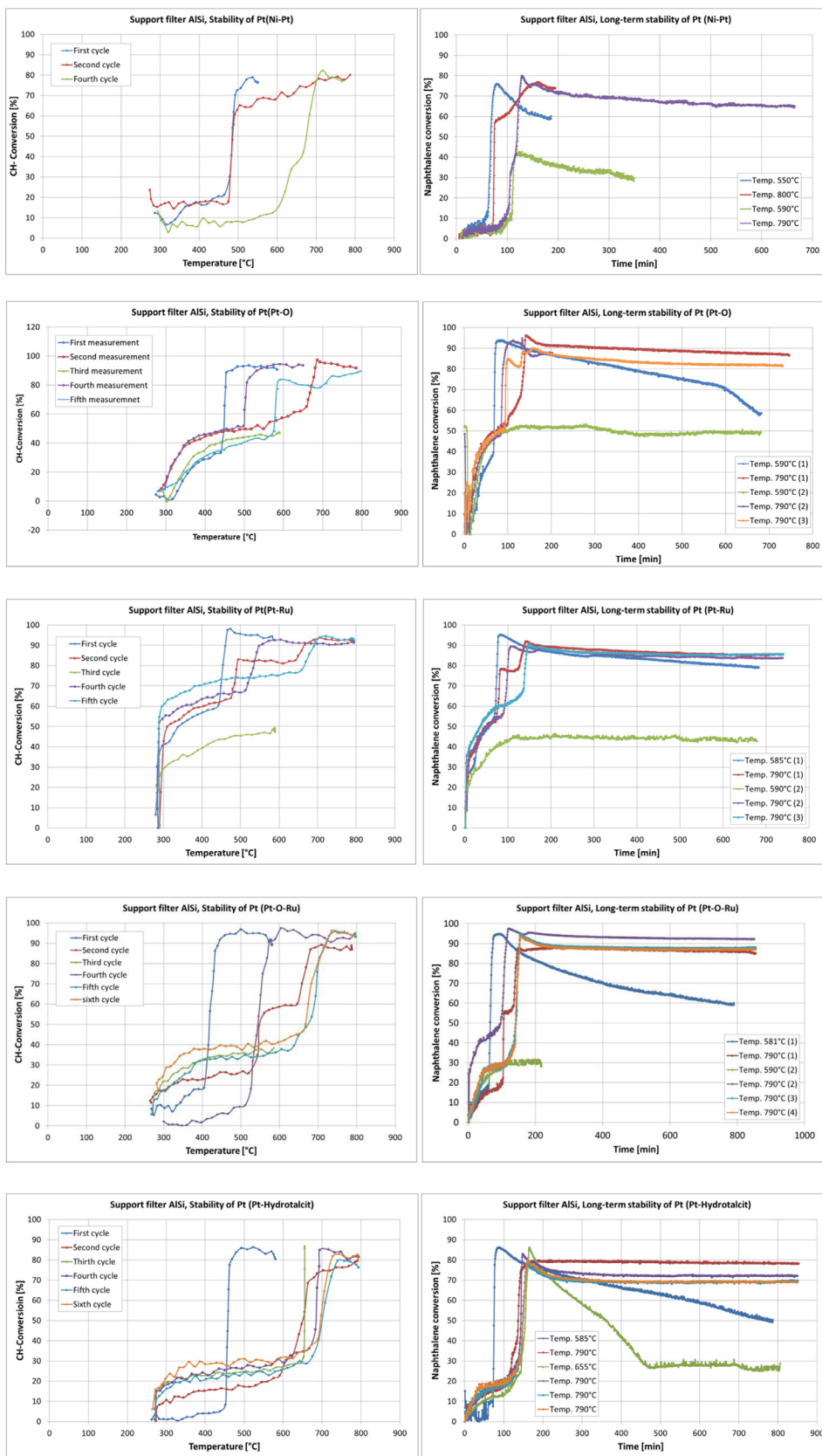
Fig. 12. Hydrocarbon conversion over catalysts (AlSi-Cat43-Pt (Ni-Pt), AlSi-Cat43-Pt (Pt-O), AlSi-Cat43-Pt (Pt-Ru), AlSi-Cat43-Pt (Pt-O-Ru), AlSi-Cat43-Pt (Pt-HYD)), light-off temperature (left), naphthalene conversion over the same catalysts, long-term catalytic activity (right).

Table 4
Shifting of the light-off temperature of the catalysts after 5–6 cycles.

Catalysts	Light-off temperature [°C]
AlSi-Cat43-Pt	449 → 653
AlSi-Cat43-Pt (Ni-Pt)	485 → 683
AlSi-Cat43-Pt (Pt-O)	450 → 670
AlSi-Cat43-Pt (Pt-Ru)	454 → 678
AlSi-Cat43-Pt (Pt-O-Ru)	420 → 702
AlSi-Cat43-Pt (Pt-HYD)	457 → 705

Nevertheless, after 5–6 heating cycles, the light-off temperature of all catalysts was shifted to higher temperatures, and during the third heating cycle, already every catalyst lost its high catalytic activity for CH conversion at lower temperature. When Pt or Pt-Ru were impregnated from water solution, the light-off temperature was systematically shifted with each heating cycle to a higher temperature. Gradually, the decrease in CH conversion at lower and the increase at higher temperatures could be observed. In contrast, the catalysts in which Pt and Pt-Ru were impregnated from basic EDTA solution shifted the light-off temperature and the maximum CH-conversion twice between higher and lower temperatures up to the attained stability of the light-off temperature. In this case, Pt and Pt-Ru appear to be stable at low temperatures, but still not long enough. The impregnation of Pt from hydrotalcite suspension solution deactivated the catalyst at a lower temperature and shifted its light-off temperature and maximum CH conversion rate to a higher temperature already during the second heating cycle. At the lower temperature, no stabilization of the catalyst was observed. The light-off temperature after 5–6 heating cycles for all catalysts is described in Table 4.

During each heating cycle, the long-term catalytic activities of the catalysts were investigated and the naphthalene conversion rates were measured. Results are shown in Fig. 12. At lower temperatures below 600 °C, only one catalyst (AlSi-Cat43-Pt (Pt-Ru)) reached a naphthalene conversion of around 95% which during 10 h of activity only slightly decreased by 15%. The catalyst AlSi-Cat43-Pt (Ni-Pt) initially reached only 75% and rapidly lost its catalytic activity within 10 h. All others catalysts initially reached a naphthalene conversion of 90% during the first heating cycle.

At a reaction temperature of 790 °C, all catalysts deactivated at lower reaction temperatures and significantly increased naphthalene conversion again for the tested time of 12 h. The individual maximum conversion rates of the respective catalysts were different. With respect to the naphthalene conversion rate and the stability at lower temperatures, the best results were observed for catalysts in which Pt and Pt-Ru were impregnated from basic EDTA solution. The second best with about 10% lower naphthalene conversion were catalysts in which Pt and Pt-Ru were impregnated from water solution. The two catalysts AlSi-Cat43-Pt (Ni-Pt) and AlSi-Cat43-Pt (Pt-HYD) were unstable at low temperatures and deactivated slowly progressive at higher temperatures.

It is obvious that all of these catalysts deactivate at temperatures below 500 °C after a short time on stream. The maximum activity was reached at temperatures of about 700 °C for all catalysts investigated. The addition of ruthenium significantly increases the naphthalene conversion over the entire temperature range, but does not stabilize the activity of the catalysts at lower tempera-
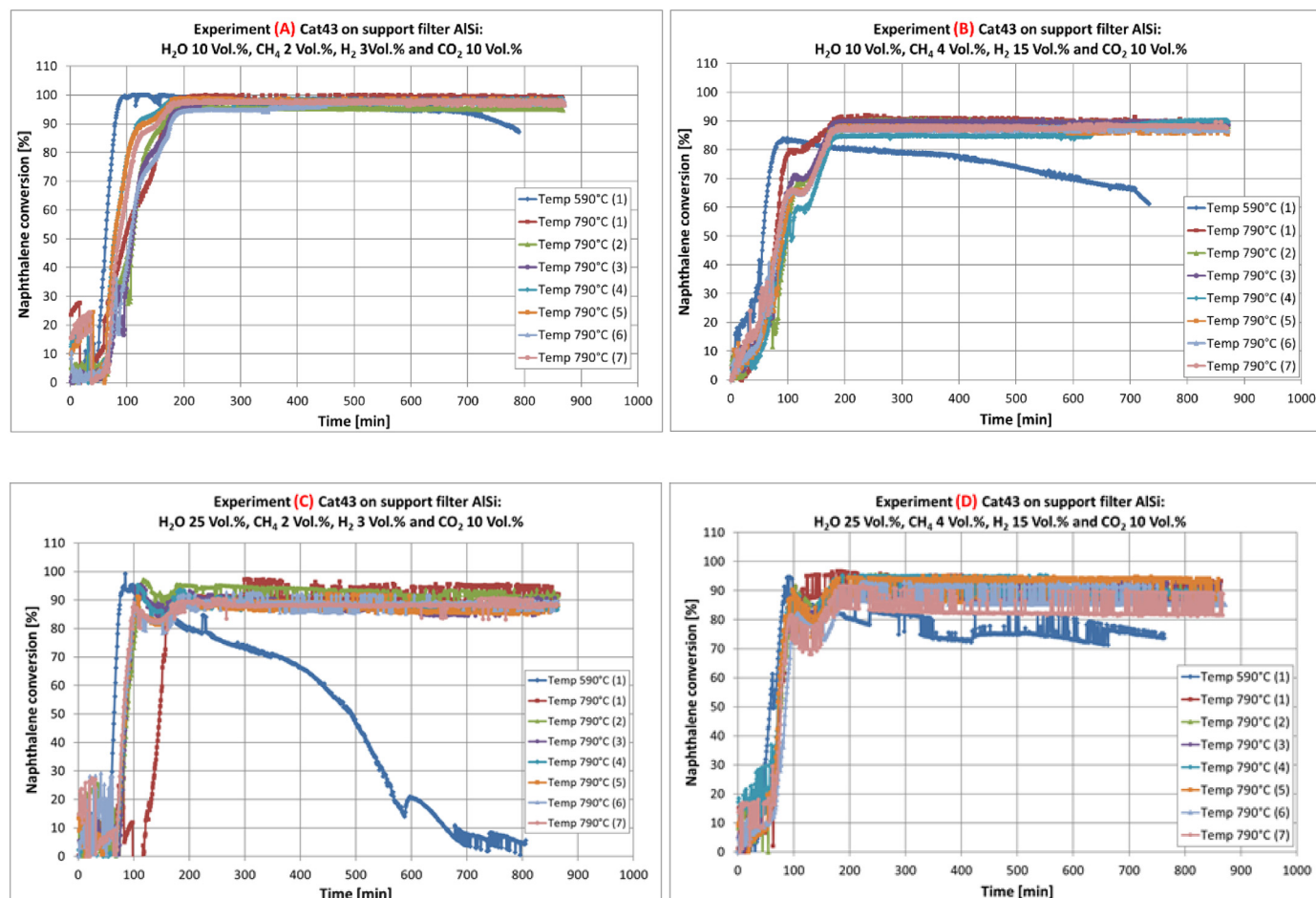

Fig. 13. Naphthalene conversions over catalytic ceramic filter discs at four different gas compositions. Long-term catalytic activity is simulated for up to eight heating cycles.
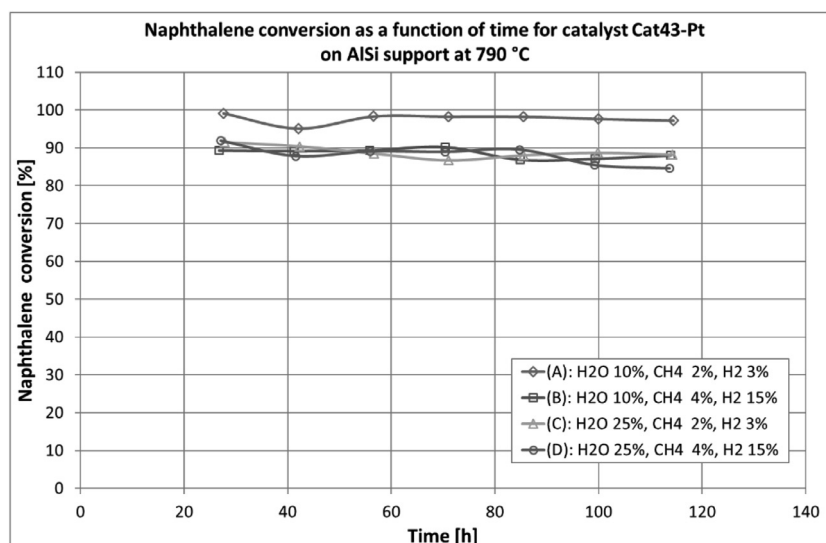
Fig. 14. Long-term activity of the catalytic filter disk for the conversion of naphthalene in four gas mixtures.

tures, which had been expected due to the strong interaction between these two noble metals[26]. However, the catalyst preparation method influenced the reactivity. It could be seen that the catalysts prepared from EDTA basic solution during second impregnation were more stable and active.

3.2.3. Catalyst behavior at different gas compositions

The influence of different concentrations of H_2O, CH_4, and H_2 on the catalytic tar conversion over catalytically coated filter discs (AlSi-Cat43-Pt) was investigated for four gas compositions, referred to as A, B, C, and D (see Table 3). The light-off temperatures and long-term activities of the catalyst were determined in each case at eight ramping temperature cycles. The analyzed gas composition was not representative of all gasification processes, but only of the counter-current gasifier with attached partial oxidation unit (POX) for which the investigation on catalytic filters was carried out. Due to POX, this type of gasifier achieves a tar content of about 5 g/Nm³, up to 7 vol% of CH_4 and 15 vol% of H_2. Therefore, the experiments were also realized at a low concentration of H_2O, CH_4, and H_2.

The light-off temperature of the catalyst in the initial heating cycle was about 455 °C for all of the four experiments. Nevertheless, after the first two (at 25 vol% H_2O) or four to five (at 10 vol% H_2O) heating cycles, the light-off temperatures in four experiments were shifted to higher temperatures and again the catalyst remained catalytically active at a temperature of about 700 °C (see Fig. 13). The influence of the water and hydrogen contents was clearly visible. Due to the lower H_2O concentration, the catalyst slowly lost its activity at lower temperatures until it worked stably at 740 °C. A higher H_2 concentration stabilized a faster catalytic activity of the catalyst at lower water content. In contrast, by a higher H_2O concentration, the maximum stable catalytic activity was achieved very rapidly and at a temperature of less than 700 °C. In this case, again the catalysts were deactivated at a lower temperature. We assume that this behavior is related only to Pt deactivation and Ni activity. The deactivation of the platinum was probably due to blockage of active Pt sites by condensation of coke or organic compounds. Takanabe at al. [27] had observed the same effect of deactivation of the Pt/ZrO_2 catalyst during steam reforming of acetic acid due to blockage of active sites by the coke/oligomer formed.

Resuming these results, it is obvious that after 115 h on stream, Cat43-Pt remained active for naphthalene conversion in all four gas mixtures. Only very slight deactivation was observed in the case of gas compositions A and D. An almost 100% naphthalene conversion was achieved only in gas composition A, almost 90% in gas compositions B and C, and only 85% in gas composition D (see Fig. 14).

The analysis of the measurements during these four experiments provides further information on the influence of H_2O and H_2 on the composition of the product gas after the conversion of naphthalene. During the catalytic reaction, H_2 is consumed in the ring opening of polycyclic hydrocarbons and also in the reverse water-gas shift reaction ($CO_2 + H_2 \rightarrow CO + H_2O$) or even Bosch reaction ($CO_2 + 2 H_2 \rightarrow C + 2 H_2O$), which always runs in parallel. In all of the four experiments, the naphthalene and its by-products were converted on the order of at least 85%. However, during the long-term tests, organic compounds such as xylene were always formed after 20 h on stream, and by-products of naphthalene reforming such as toluene and benzene were not completely converted. If the gas mixture contains more H_2, more CO and more xylene are formed. A high water content suppressed the production of CO, but not that of xylene.

4. Conclusions

As results from the investigations performed with AlSi-supported catalysts and SiC-supported catalysts, the AlSi support material seems more suitable than SiC with respect to reaction stability and activity. The same amount of catalyst could be distributed more uniformly over the AlSi support material. The wet impregnation method proved to be appropriate as a method for catalyst implementation in AlSi fiber composite ceramic candles.

Below 600 °C, AlSi-supported catalysts were catalytically active for about 20 h with a naphthalene conversion of up to 50%. The catalytic activity increased significantly at temperatures of about 700 °C for more than 95 h providing a naphthalene conversion of more than 90% (AlSi-Cat44-Pt) without de-activation. Moreover, the addition of a second noble metal (ruthenium) enhances the catalysts´activity for naphthalene conversion at temperatures of about 700 °C. The reactivity is also influenced by the catalyst preparation method. The noble metal impregnation prepared with EDTA basic solution during the second impregnation step is more stable in the relevant temperature range.

The vapor and gas compositions have a visible influence on the catalytic activity of the filter elements. The naphthalene conversion of almost 100% (AlSi-Cat43-Pt) was estimated at a low concentra-

tion of water (10 vol%) and hydrogen (3 vol%). Nonetheless, the catalytic filter material was catalytically active at 790 °C in all tested gas compositions with only very little deactivation for 115 h.

Implementation of the noble metal in the Ni-based catalyst proved to be necessary for the tar reforming reaction in order to achieve operating temperatures considerably below 800 °C.

The respective application of the wet impregnation method to full-size AlSi ceramic filter candles and the calcination of the impregnated filter elements have to be further investigated at KIT.

Declaration of Competing Interest

The authors declare that they have no known competing financial interests or personal relationships that could have appeared to influence the work reported in this paper.

Acknowledgments

References

[1] Kumar A, Jones DD, Hanna MA. Thermochemical biomass gasification: a review of the current status of the technology. Energies 2009;2:556–81.

[2] Vreugdenhil BJ, Zwart RWR. Tar formation in pyrolysis and gasification, Status Report. Energy research Centre of the Netherlands (ECN); 2009. , ECN-E–08-087.

[3] Woolcock PJ, Brown RC. A review of cleaning technologies for biomass-derived syngas. Biomass Bioenergy 2013;52:54–84.

[4] Sikarwar VS, Zhao M, Clough P, Yao J, Zhong X, Memon MZ, et al. An overview of advances in biomass gasification. Energy Environ Sci 2016;9:2939–77.

[5] Devi L, Ptasinski KJ, Janssen FJJG. A review of the primary measures for tar elimination in biomass gasification processes. Biomass Bioenergy 2013;24:125–40.

[6] Zwart RWR. Gas cleaning downstream biomass gasification, Status Report. Energy research Centre of the Netherlands (ECN); 2009. , ECN-E–08-078.

[7] Nacken M, Ma L, Engelen K, Heidenreich S, Baron GV. Development of a tar reforming catalyst for integration in a ceramic filter element and use in hot gas cleaning. Ind Eng Chem Res 2007;46:1945–51.

[8] Engelen K, Zhang Y, Baron GV. Development of a catalytic candle filter for one-step tar and particle removal in biomass gasification gas. Int J Chem Reactor Eng 2003;1 Article A 29.

[9] Park HJ, Park SH, Sohn JM, Park J, Jeon J-K, Kim S-S, et al. Steam reforming of biomass gasification tar using benzene as a model compound over various Ni supported metal oxide catalysts. Bioresour Technol 2010;101:S101–3.

[10] Miyazawa T, Kimura T, Nishikawa J, Kado ShSH, Kunimori K, Tomishige K. Catalytic performance of supported Ni catalysts in partial oxidation and steam reforming of tar derived from the pyrolysis of wood biomass. Catal Today 2006;115:254–62.

[11] Brillis AA, Manos G. Catalyst deactivation during catalytic cracking of n-octane, isobutene and 1-octane over USHY Zeolite at mild conditions and short time on stream. Stud Surf Catal 2001;139:255–69.

[12] Aguero FN, Barbero BP, Pereira MF, Figueiredo JL, Cadus LE. Mixed platinum–manganese oxide catalysts for combustion of volatile organic compounds. Ind Eng Chem Res 2009;48:2795–800.

[13] Diehl F, Barbier J Jr, Duprez D, Guibard I, Mabilion G. Catalytic oxidation of heavy hydrocarbons over Pt/Al_2O_3. Influence of the structure of the molecule on its reactivity. Appl Catal B 2010;95:217–27.

[14] Ferella F, Stoehr J, De Michelis I, Hornung A. Zirconia and alumina based catalysts for steam reforming of naphthalene. Fuel 2013;105:614–29.

[15] Keil FJ. Complexities in modeling of heterogeneous catalytic reactions. Comput Math Appl 2013;65:1674–97.

[16] Forzatti P, Lietti L. Catalyst deactivation. Catal Today 1999;52:165–81.

[17] Yeh T, Linic S, Savage PhE. Deactivation of Pt catalysts during hydrothermal decarboxylation of butyric acid. Sustain Chem Eng 2014;2:2399–406.

[18] Stöcklmayer Ch, Höflinger W. Simulation of the filtration behavior of dust filters. Simul Pract Theory 1998;6:281–96.

[19] Lee S, Keskar G, Liu ChH, Schwartz WR, McEnally ChS, Kim J-Y, et al. Deactivation characteristics of Ni/CeO_2-Al_2O_3 catalyst for cyclic regeneration in a portable steam reformer. Appl Catal B 2012;111-112:157–64.

[20] Hashemnejad SM, Parvari M. Deactivation and regeneration of Nickel-based catalysts for steam-Methane reforming. Chin J Catal 2011;32:273–9.

[21] Vivanpatarakij S, Rulerk D, Assabumrungrat S. Removal of tar from biomass gasification process by steam reforming over nickel catalysts. Chem Eng Trans 2014;37:205–10.

[22] Guan G, Kaewpanha M, Hao X, Abudula A. Catalytic steam reforming of biomass tar: prospects and challenges. Renew Sustain Energy Rev 2016;58:450–61.

[23] Ide MS, Falcone DD, Davis RJ. On the deactivation of supported platinum catalysts for selective oxidation of alcohols. J Catal 2014;311:295–305.

[24] Caballero MA, Corella J, Aznar M-P, Gil J. Biomass gasification with air in fluidized bed. Hot gas cleanup with selected commercial and full-size nickel-based catalysts. Ind Eng Chem Res 2000;39:1143–54.

[25] Sato K, Shinoda T, Fujimoto K. New nickel-based catalyst for tar reforming, with superior resistance to coking and sulfur poisoning in biomass gasification processes. J Chem Eng Jpn 2007;40:860–8.

[26] Bhagiyalakshmi M, Anuradha R, Park SD, Park TS, Cha WS, Jang HT. Effect of bimetallic Pt-Rh and trimetallic Pt-Pd-Rh catalysts for low temperature catalytic combustion of methane. Bull Korean Chem Soc 2010;31:120–4.

[27] Takanabe K, Aika K, Seshan K, Lefferts L. Catalyst deactivation during steam reforming of acetic acid over Pt/ZrO_2. Chem Eng J 2006;120:133–7.